

Training Quantum Boltzmann Machines with the β -Variational Quantum Eigensolver

Onno Huijgen,^{1,*} Luuk Coopmans,^{2,†} Peyman Najafi,¹ Marcello Benedetti,² and Hilbert J. Kappen¹

¹*Radboud University, Nijmegen, The Netherlands*

²*Quantinuum, Partnership House, Carlisle Place, London SW1P 1BX, United Kingdom*

(Dated: April 17, 2023)

The quantum Boltzmann machine (QBM) is a generative machine learning model for both classical data and quantum states. The training of the QBM consists of minimizing the relative entropy from the model to the target state. This requires QBM expectation values which are computationally intractable for large models in general. It is therefore important to develop heuristic training methods that work well in practice. In this work, we study a heuristic method characterized by a nested loop: the inner loop trains the β -variational quantum eigensolver (β -VQE) by Liu et al. [1] to approximate the QBM expectation values; the outer loop trains the QBM to minimize the relative entropy to the target. We show that low-rank representations obtained by β -VQE provide an efficient way to learn low-rank target states, such as classical data and low-temperature quantum tomography. We test the method on both classical and quantum target data with numerical simulations of up to 10 qubits. For the cases considered here, the obtained QBMs can model the target to high fidelity. The approach offers a valuable route towards variationally training QBMs on near-term quantum devices.

I. INTRODUCTION

The study of quantum information technologies has shown to be a fruitful discipline for the discovery of novel algorithms and computing applications. It is expected that quantum algorithms will outperform their classical counterparts on several tasks of practical relevance, such as factoring large prime numbers and simulating quantum many-body systems. Over the last decade, scientists have been exploring if quantum algorithms can also offer advantages in machine learning. While this has been answered in the affirmative [2, 3], the theoretical performance benefits will materialize only when large-scale fault-tolerant quantum computers become available.

In the context of near-term quantum computing, a plethora of variational quantum algorithms (VQAs) for machine learning tasks have been investigated [4–6]. In VQAs, one solves the computational problem by choosing an ansatz, typically a parameterized quantum circuit, and then optimizes its parameters with respect to a suitable objective function. Applications of VQAs include finding ground states of small molecules, combinatorial optimization, classification, and generative modeling.

In this paper, we continue this line of research and propose a VQA for training quantum Boltzmann machines (QBMs) [7, 8]. QBMs are generative models inspired by quantum Ising models from physics and can be used for both classical and quantum data. In QBM training, the goal is to find the weights of a Hamiltonian ansatz, such that its thermal state best approximates the target density matrix [9, 10]. The QBM training depends on the ability to prepare and compute properties of a thermal state, which is intractable in general [11]. It is therefore

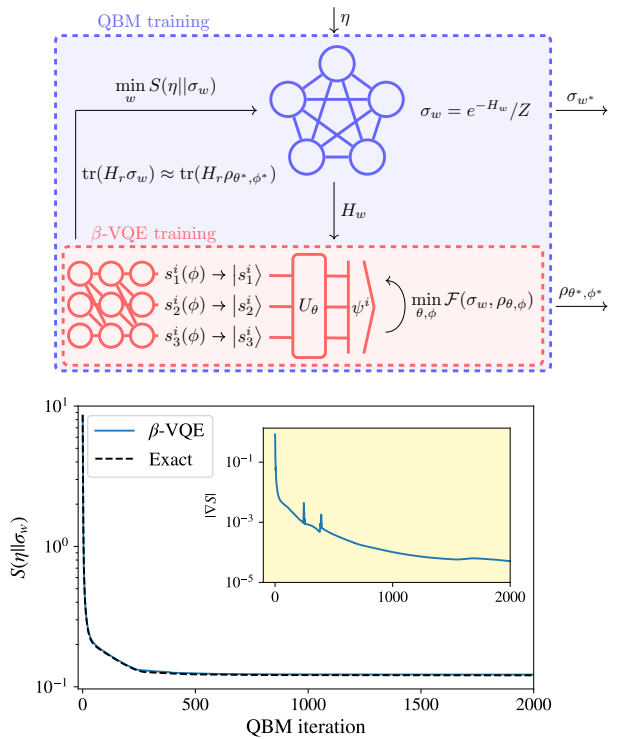


FIG. 1. Top: Illustration of the nested-loop algorithm for training a QBM. In the outer loop (blue box) we optimize the relative entropy S from the QBM model σ_w to the target η . This step utilizes an approximation to the QBM statistics, $\text{tr}(H_r \sigma_w) \approx \text{tr}(H_r \rho_{\theta^*, \phi^*})$, which is provided by the inner loop (red box). In the inner loop we optimize the variational free energy \mathcal{F} of the β -VQE ansatz $\rho_{\theta, \phi}$ with the QBM Hamiltonian H_w . At the end of training we output the QBM model and its β -VQE approximation. Bottom: Convergence of the QBM training on classical salamander retina data using the nested-loop algorithm compared to exact gradient computation of the QBM. The nested-loop algorithm closely approximates exact gradient optimization in this setting.

* o.huijgen@donders.ru.nl

† luuk.coopmans@quantinuum.com

key to develop efficient heuristic methods that work well in practice; indeed, even classical Boltzmann machines are intractable and must be trained by efficient heuristics such as contrastive divergence [12]. In this work, we employ the recently proposed β -variational quantum eigensolver [1] (β -VQE) to approximate the QBM properties.

β -VQE represents a mixed density matrix as a combination of a classical probability distribution and a parameterized quantum circuit. Computational basis states are randomly sampled and used as input for the circuit, where they are unitarily transformed into quantum states. β -VQE has been experimentally demonstrated on a superconducting quantum computer [13]. The purpose of our work is to provide evidence that β -VQE can be successfully exploited for the training of QBMs on classical and quantum data sets to high accuracy. The algorithm is illustrated in Fig. 1 along with some empirical results on a classical data set.

Several other techniques have been proposed for QBM training: quantum annealing [8], variational imaginary time evolution [14], the eigenstate thermalization hypothesis [15], pure thermal shadows [16], and others [17, 18]. Most of these approaches have not been demonstrated as they require a fault-tolerant quantum computer [15–18]. On the other hand, the few approaches that have been demonstrated on real hardware [8, 14] incur a significant overhead in terms of ancilla qubits. Remarkably, the approach studied here is near-term and uses the same number of qubits as the number of variables in the data set.

We equip the algorithm with additional features and rules of thumb that reduce the overall computational cost. Firstly, it is possible to use a limited number of computational basis states in β -VQE, yielding a low-rank approximation. We provide evidence that this is especially useful for classical target data. Secondly, since small updates in parameter space during QBM training lead to small steps in density matrix space, we introduce a natural warm-start strategy for β -VQE. We observe that warm-start yields faster convergence, possibly avoiding barren plateaus by keeping the solution close to the local minimum at all times. Finally, we find that a circuit depth scaling linearly with the system size is sufficient to get accurate results. For the dataset we use, the β -VQE approximation resulted in a difference in fidelity of $\mathcal{O}(10^{-4})$ compared QBM training using the exact gradient, regardless of system size, suggesting that this method is scalable.

The remainder of this paper is structured as follows. In Section II A we introduce the QBM and the training algorithm based on β -VQE. In Section III we show the exact numerical simulation results and analyze the number of samples and quantum fidelity. We also shortly discuss the performance of the β -VQE when using a sampled gradient with a fixed amount of shots. In Section IV we present the conclusions of our work.

II. METHODS

A. Quantum Boltzmann machines

The QBM [7, 8] is defined as the n -qubit mixed density matrix (Gibbs state)

$$\sigma_w = \frac{e^{-\beta H_w}}{Z}, \quad (1)$$

with $Z = \text{Tr}(e^{-\beta H_w})$ the partition function, $\beta > 0$ the fixed inverse temperature and H_w a parameterized Hamiltonian. In this work, we consider Hamiltonians of the form

$$H_w = \sum_r w_r H_r, \quad (2)$$

which consists of a sum of a polynomial number of non-commuting qubit-operators H_r with weights w_r . The specific form of the operators H_r does not matter at this point and will be given in the result section below. The quantum Hamiltonian H_w generalizes the role of the energy function in a classical Boltzmann machine [19].

In order to find the optimal weights w^* , we aim to minimize the quantum relative entropy

$$S(\eta\|\sigma_w) = \text{Tr}(\eta \log \eta) - \text{Tr}(\eta \log \sigma_w) \quad (3)$$

from σ_w to the target density matrix η [9, 10]. This information-theoretic measure generalizes the classical Kullback-Leibler divergence to density matrices and has nice properties for the QBM model ansatz, e.g., the logarithm cancels the exponential in Eq. (1). The target η is either some quantum system with unknown Hamiltonian H_t at finite temperature, i.e., $\eta = \frac{e^{-\beta_t H_t}}{Z_t}$, or a classical data set *embedded* into a quantum state. There are various ways to do this embedding, but the one we use here is the pure-state embedding presented in [10]. In this method, we are given a data set $\{\mathbf{s}^\lambda\}_{\lambda=1}^N$ consisting of N bitstrings of length n , and we construct the empirical probability distribution $p(\mathbf{s}) = \frac{1}{N} \sum_\lambda \delta_{\mathbf{s}, \mathbf{s}^\lambda}$. Then the rank-1 target density matrix is given by $\eta = \sum_{\mathbf{s}, \mathbf{s}'} \sqrt{p(\mathbf{s})p(\mathbf{s}')} |\mathbf{s}\rangle\langle \mathbf{s}'|$.

The optimization of $S(\eta\|\sigma_w)$ can be done with gradient descent. By noticing that only the second term in Eq. (3) depends on w_r , and using Duhamel's formula for the derivative of a matrix exponential [20], we obtain the partial derivatives

$$\frac{\partial S}{\partial w_r} = \text{tr}(H_r \eta) - \text{tr}(H_r \sigma_w). \quad (4)$$

Similar to the classical case [19], the gradient is given by the difference between statistics under the data density matrix η and the model density matrix σ_w . The data statistics do not change during training and need to be obtained only once. However, the QBM statistics change after every iteration of gradient descent and must

be recomputed. The QBM density matrix σ_w is given by the matrix exponential of the Hamiltonian, whose dimension scales exponentially in the number of quantum spins. This means that computing the full density matrix becomes computationally intractable for larger system sizes.

While the classical BM has the same exponential scaling of the number of states, there exist several approximation algorithms that can effectively compute the necessary statistics, often based on Markov-chain Monte Carlo [21]. However, for quantum systems, no general MCMC methods exist due to the negative sign problem for non-stoquastic models [22, 23]. Since the QBM is not restricted to the stoquastic domain and can include spin glass models, quantum Monte Carlo is not an option in general. In the following section, we review the β -VQE method that with help of a quantum computer can be used to potentially circumvent this issue.

B. β -VQE

Recently, Liu et al. [1] proposed a variational method to represent a mixed density matrix called β -VQE. It combines a classical network with a quantum circuit (Fig. 1) into a parameterized density matrix ansatz given by

$$\rho_{\theta,\phi} = \sum_{\mathbf{s}} p_{\phi}(\mathbf{s}) U_{\theta} |\mathbf{s}\rangle\langle\mathbf{s}| U_{\theta}^{\dagger}. \quad (5)$$

$p_{\phi}(\mathbf{s})$ is a parameterized probability distribution over binary states implemented by a classical network, e.g., a parameterized Bernoulli distribution or an autoregressive network [24]. The binary states are then used as inputs for a parameterized quantum circuit U_{θ} , which transforms them into quantum states. The combined system $\rho_{\theta,\phi}$ can accurately represent finite-temperature Gibbs states of quantum spin systems, e.g., see Ref. [1]. Here we aim to see if it can be used for the wide range of Hamiltonians needed to train the QBM on quantum and classical data.

The optimal parameters of $\rho_{\theta,\phi}$ for a fixed QBM Hamiltonian H_w are found by minimizing the variational free energy

$$\mathcal{F}(\sigma_w, \rho_{\theta,\phi}) = \text{Tr}(\rho_{\theta,\phi} \log \rho_{\theta,\phi}) + \text{Tr}(\rho_{\theta,\phi} H_w). \quad (6)$$

This is equivalent to minimizing the quantum relative entropy from σ_w to $\rho_{\theta,\phi}$. The minimization can be done with gradient descent on the classical network and quantum circuit parameters simultaneously. The required gradients [1] are given by

$$\nabla_{\theta} \mathcal{F} = \sum_{\mathbf{s}} p_{\phi}(\mathbf{s}) \left[\nabla_{\theta} \langle \mathbf{s} | U_{\theta}^{\dagger} H_w U_{\theta} | \mathbf{s} \rangle \right], \quad (7)$$

for the circuit, and for the classical network

$$\nabla_{\phi} \mathcal{F} = \sum_{\mathbf{s}} p_{\phi}(\mathbf{s}) [(f(\mathbf{s}) - b) \nabla_{\phi} \log p_{\phi}(\mathbf{s})], \quad (8)$$

where a control variate is used to reduce the variance as in [1]: $f(\mathbf{s}) = \ln p_{\phi}(\mathbf{s}) + \langle \mathbf{s} | U_{\theta}^{\dagger} H_w U_{\theta} | \mathbf{s} \rangle$ and $b = \sum_{\mathbf{s}} p_{\phi}(\mathbf{s}) f(\mathbf{s})_{p_{\phi}}$. We recognize that the gradient w.r.t. the circuit parameters, Eq. (7), reduces to a parameter shift rule: a weighted sum of energy expectation values

$$\nabla_{\theta} \langle \mathbf{s} | U_{\theta}^{\dagger} H_w U_{\theta} | \mathbf{s} \rangle = \frac{1}{2} \left[\langle \mathbf{s} | U_{\theta+\frac{\pi}{2}}^{\dagger} H_w U_{\theta+\frac{\pi}{2}} | \mathbf{s} \rangle - \langle \mathbf{s} | U_{\theta-\frac{\pi}{2}}^{\dagger} H_w U_{\theta-\frac{\pi}{2}} | \mathbf{s} \rangle \right]. \quad (9)$$

Computation of the gradient is tractable on a quantum computer if the sum is approximated by sampling a polynomial number of bitstrings from $p_{\phi}(\mathbf{s})$, and if there is no barren plateau in the optimization landscape [25]. The gradient w.r.t. the parameters of the classical network, Eq. (8), has the form of a standard weighted entropy gradient, which for classical networks can be efficiently approximated from sampling [26].

C. Truncated-rank β -VQE

We propose a slight modification of the sampling approach for the gradients originally presented in [1]. Instead of randomly sampling from all computational basis states, we choose the R states with the highest probability and renormalize p_{ϕ} on those states. This results in a β -VQE density matrix of rank R

$$\rho_{\theta,\phi} = \frac{1}{\sum_{k=i_1}^{i_R} p_{\phi}(\mathbf{s}_k)} \sum_{j=i_1}^{i_R} p_{\phi}(\mathbf{s}_j) U_{\theta} |\mathbf{s}_j\rangle\langle\mathbf{s}_j| U_{\theta}^{\dagger}. \quad (10)$$

In the following, we refer to this as truncated-rank β -VQE. As an immediate consequence, the gradients for the variational free energy Eqs. (7) and (8) are also truncated for this model. This means that we can heuristically choose a small R so that the optimization can be performed at a reduced computational cost.

D. Training QBMs with the nested-loop algorithm

We now describe the nested-loop algorithm to train a QBM with a truncated rank β -VQE. Recall that the aim is to train the QBM so that it resembles some target data embedded in η . This is schematically shown in Figure 1. The algorithm starts with a simple ansatz for the QBM Hamiltonian H_w , e.g., a Heisenberg XXZ model or a random spin-glass model. In the *inner loop*, the β -VQE ansatz $\rho_{\theta,\phi}$ is trained to represent the QBM σ_w by minimizing Eq. (6). In the *outer loop*, $\rho_{\theta,\phi}$ is used to compute approximate QBM statistics $\text{tr}(H_r \sigma_w) \approx \text{tr}(H_r \rho_{\theta^*,\phi^*})$. These are used for training the QBM by gradient descent on Eq. (3).

Since H_w changes only slightly between two QBM iterations, we use a warm-start strategy for the parameters θ, ϕ of the β -VQE ansatz $\rho_{\theta,\phi}$ between the steps of the outer loop. We reuse the converged parameters of $\rho_{\theta,\phi}$

in one β -VQE inner loop as the initial parameters for the next β -VQE inner loop. Hence, while the β -VQE has to run for a relatively long time in the first inner loop, we find that it converges much faster in subsequent iterations.

The total number of statistic estimations of the nested-loop algorithm is of order

$$\mathcal{O}(n_{\text{QBM}} \times n_{\beta\text{-VQE}} \times R \times n_{\theta}). \quad (11)$$

Here n_{QBM} is the number of QBM iterations for convergence to some fixed accuracy, $n_{\beta\text{-VQE}}$ the number of β -VQE iterations, R the rank of the β -VQE, and n_{θ} the number of circuit parameters.

III. NUMERICAL RESULTS

Using the nested-loop algorithm, we train QBMs on both classical and quantum data. We use the Hamiltonian ansatz

$$H_w = \sum_{k \in \{x, z\}} \sum_{i=1}^n w_i^k \sigma_i^k + \sum_{k \in \{x, y, z\}} \sum_{i < j} \tilde{w}_{i,j}^k \sigma_i^k \sigma_j^k, \quad (12)$$

where w and \tilde{w} are weights, and σ_i^k is the n -qubit Pauli operator acting on qubit i . We initialize the weights randomly from a normal distribution with mean 0 and standard deviation $\frac{1}{\sqrt{n}}$. The weights are trained in the outer loop using gradient descent with a momentum parameter $\alpha = \frac{1}{2}$ [28]. The ansatz taken for H_w determines the precise models that the QBM is capable of representing. Not every state in the Hilbert space can be represented by this ansatz. Therefore, there might be target data that can not be exactly modeled. We define this as a model mismatch.

For the β -VQE, we implement the classical network p_{ϕ} with a variational auto-encoder (VAE) [24] made of a hidden layer of 50 neurons. For the quantum circuit U_{θ} , we use a checkerboard pattern of general $SU(4)$ unitaries with periodic boundary conditions. One layer of this ansatz is shown in Fig. 2(a). Each $SU(4)$ unitary is implemented via a decomposition into CNOT gates and single-qubit rotations following [27]. This is illustrated in Fig. 2(b). We define the circuit depth d as the number of repetitions of such a layer. This gives a total number of circuit parameters $n_{\theta} = 15 \times d \times n$. We determine the optimizer settings, e.g., the learning rate, for each target data set separately, and give them below. As the stopping criterion for the inner loop, we use a target precision ϵ on the β -VQE gradient (Eqs. (7) and (8)). In addition, we also set a maximum number of iterations $n_{\beta\text{VQE}}^{\text{max}} = 2000$ for the inner loop, in order to avoid very long convergence times. We now show that with these settings we are able to train QBMs to high accuracy on both classical and quantum data.

A. Classical data results

We consider a classical data set taken from spiking neurons in the salamander retina [29] described in more detail in Appendix A. As discussed above, the classical data is embedded into a pure state η . We first show that the nested-loop algorithm can be used to train the QBM to high accuracy for a system of $n = 8$ qubits. In Fig. 1(b) we show the convergence of the relative entropy from the QBM to the target during training. We observe that $S(\eta \parallel \sigma_w)$ decreases monotonically and saturates at a value of order $\mathcal{O}(10^{-1})$. This is close to the value obtained from learning with the exact gradient (dashed line). In the inset, we show that the norm of the gradient is $\mathcal{O}(10^{-5})$.

Next, we investigate some important aspects of the learning algorithm, starting with the rank used in the truncated-rank β -VQE inner loop. The specific fidelity measure we use for this is the Uhlmann-Jozsa fidelity between the β -VQE and the target state, given by

$$F(\eta, \rho) = \text{Tr} \left(\sqrt{\sqrt{\eta} \rho \sqrt{\eta}} \right)^2. \quad (13)$$

This fidelity satisfies all of Jozsa's axioms, described in [30]. Importantly, fidelity is an intensive property, as opposed to relative entropy. Thus it is a useful measure for comparing performance on different system sizes.

In Fig. 3 we show the fidelity between the different states obtained at the end of our algorithm. The fidelity between the QBM and η , indicated by the blue crosses increases substantially with increased β -VQE rank, even though the target is a pure state. This might seem counter-intuitive but is a direct result of the low-rank approximation of the gradient. For a very low rank β -VQE, the approximation to the gradient becomes vanishingly small once the ground state accurately approximates the target pure state. During that stage, the exact σ_w is still very mixed, but the gradient is approximated as if it were close to a pure state. Conversely, when a higher rank approximation is used, the gradient is still nonzero even if the ground state of σ_w closely resembles the data pure state, allowing the QBM to converge further towards a pure state. Convergence of the QBM towards a pure state has been explored in [10]. It has been shown that later training iterations tend to increase the magnitude of the weights, akin to lowering the effective temperature of the QBM. During this phase, the ground state of the QBM, ψ_w^0 , already accurately represents the data target. The fidelity between the target and the ground state of the QBM is depicted in Fig. 3 by the yellow triangles. High fidelity of $F > 0.99$ is achieved with as few as two samples.

Another important aspect is the scaling of the performance of the algorithm with the number of features (qubit) n . In order to investigate this we train the QBM on subsets of the salamander retina data of different sizes. We set the circuit depth equal to the number of features, which was heuristically found to be a good rule

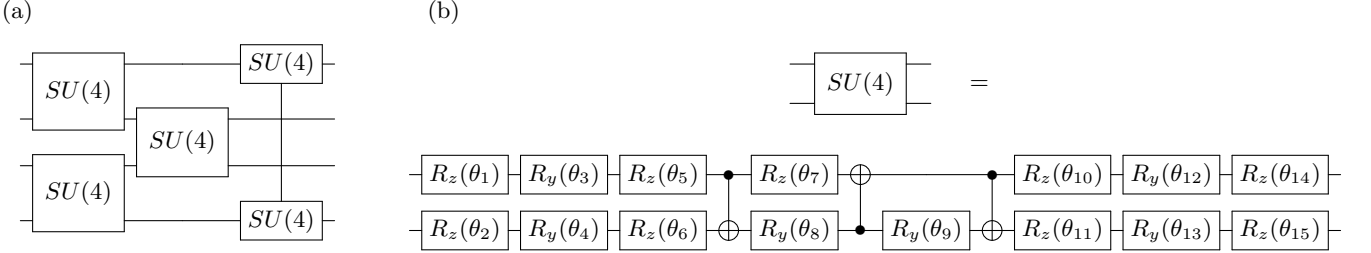


FIG. 2. Parameterized quantum circuit used for the β -VQE. (a) shows a single layer consisting of a checkerboard pattern of general $SU(4)$ unitaries with periodic boundary conditions. (b) the $SU(4)$ unitaries are decomposed into CNOT gates and single-qubit rotations as in [27].

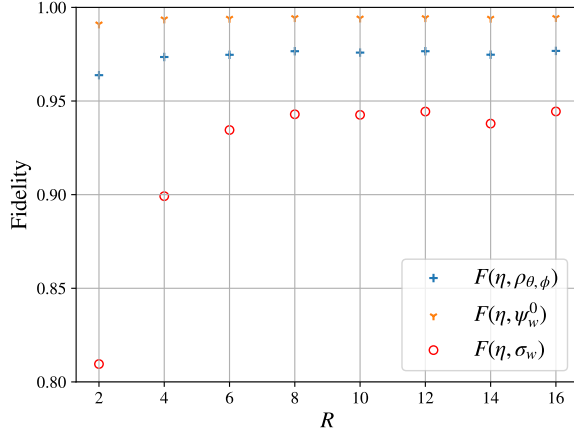


FIG. 3. Fidelity achieved with different β -VQE rank R . The β -VQE achieves fidelities > 0.96 even with small R . While the full QBM state σ_w is still mixed resulting in a lower fidelity, the ground state ψ_w^0 achieves a fidelity of > 0.99 in all cases. σ_w can be turned into a pure state by multiplying the weights by a large constant factor.

of thumb, see Appendix B. Motivated by the previous sampling analysis, we also scale the rank of β -VQE linearly with n . In Fig. 4 we show the fidelity obtained with these heuristic guidelines. The QBM trained by the nested-loop algorithm is able to obtain a fidelity of $F > 0.98$ for all system sizes studied here. Note that the fidelity decreases for larger systems. This is because of a model mismatch between the QBM and the target, as this drop is observed also in the exact QBM. A more expressive Hamiltonian ansatz, e.g., with the inclusion of third-order interaction terms, might yield more accurate results for larger system sizes.

B. Quantum data results

In our second example, we train a QBM on quantum data. As target state η we now take the finite tempera-

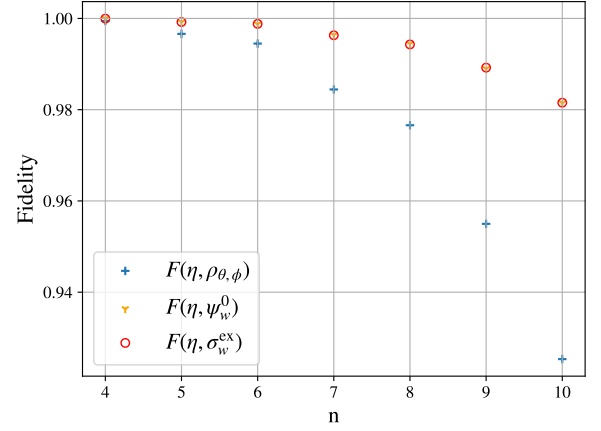


FIG. 4. Fidelity for different system sizes. For all sizes, a fidelity of $F > 0.98$ is achieved between the target state and the ground state of the QBM. The fidelity drops for larger system sizes, which is due to model mismatch between the QBM and the target.

ture Gibbs state $\eta = e^{-\beta H_{XXZ}}/Z$ with

$$H_{XXZ} = \sum_{i=1}^{n-1} J (\sigma_i^x \sigma_{i+1}^x + \sigma_i^y \sigma_{i+1}^y) + \Delta \sigma_i^z \sigma_{i+1}^z, \quad (14)$$

with $J = -1$, $\Delta = -\frac{1}{2}$, and $\beta = 1$. Quantum data taken from systems at finite temperatures is usually characterized by a high rank. However, we show that the β -VQE can be used to get an efficient low-rank approximation to the target state. We train the QBM with the nested-loop algorithm, again analyzing the effect of the rank. The results for the quantum data are shown in Fig. 5. We observe that we require a higher rank approximation to obtain a high fidelity, which is in contrast to the results for classical data shown in Fig. 3. By increasing the rank of the β -VQE, the QBM is capable of learning mixed density matrices up to arbitrary precision.

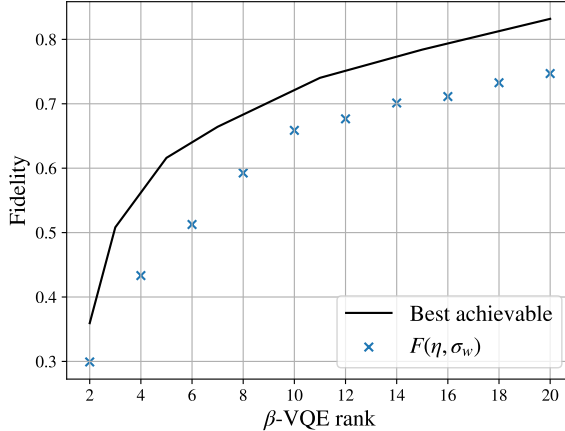


FIG. 5. Fidelity achieved between the target XXZ model η of size $n = 8$ and the QBM using the nested-loop algorithm, as a function of the rank of the β -VQE. The black line represents the fidelity between the model and an exact fixed rank approximation, and as such represents the best achievable fidelity for the corresponding fixed rank β -VQE.

C. Simulations with finite-sampling noise

All simulations in the previous sections assume access to the exact quantum state. This is possible only via classical statevector simulations which are intractable in general. To overcome this, one can execute the required circuits on a quantum computer. This introduces two new sources of error. First, the quantum computer is affected by various sources of hardware noise [31, 32]. These errors are dealt with by quantum error correction and are beyond the scope of this work. Second, the output statistics are approximate as they are always computed from a finite number of shots, i.e., measurements. This is important, for example, when estimating the gradient of β -VQE in Eq. (7). This error can always be decreased by increasing the number of shots, M . For an otherwise noiseless model, the error due to a fixed number of shots scales as $\epsilon \propto \frac{1}{\sqrt{M}}$.

As a proof of concept, we simulate QBM training under finite-sampling noise. We use a subset of the salamander retina data of size $n = 4$ and the Hamiltonian ansatz given in Eq. (12). For β -VQE we truncate the rank to $R = 2$ and use the circuit in Fig. 2 with a depth of $d = 2$. The convergence of the nested-loop algorithm under a fixed amount of shots is shown in Fig. 6. From the bottom panel, it is clear that the QBM converges until the magnitude of the error introduced by the β -VQE is approximately the same size as the gradient itself. Further optimization may be done by choosing the number of shots adaptively based on the gradient size. This may significantly improve the results for the noiseless case. However, physical quantum hardware always introduces additional errors. The specifics will depend on the hard-

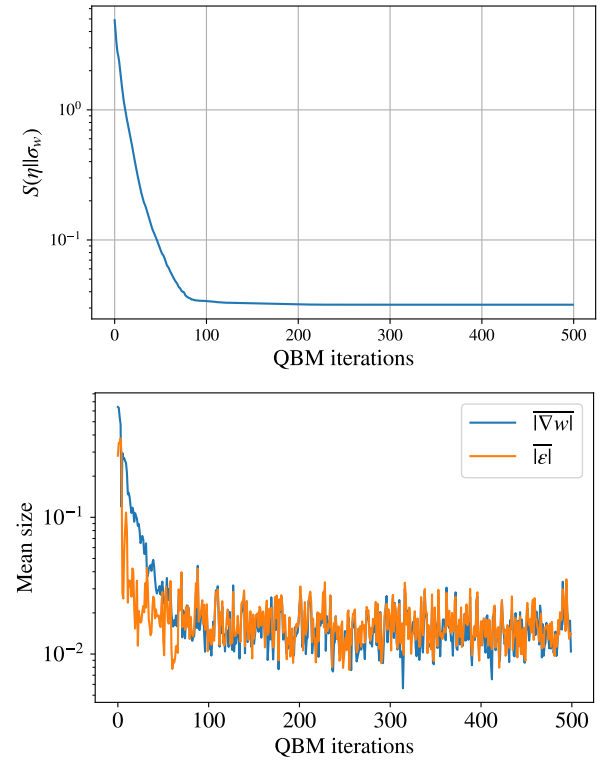


FIG. 6. Top: Relative entropy from the QBM to the salamander retina target using $R = 2$ and a depth $d = 2$ on a noiseless hardware simulation of $n = 4$ qubits. The number of shots is fixed to 5000 for both the gradient estimation of the β -VQE and the QBM. A fidelity of $F = 0.966$ is achieved. Bottom: The mean size $|\nabla S|$ of the QBM gradient (blue) and the mean size of the error introduced by the β -VQE ϵ approximation (orange). The QBM converges until the error introduced by the β -VQE becomes the dominant factor of the gradient. The error decreases initially but finally fluctuates around $\frac{1}{\sqrt{5000}} \approx 0.14$ as expected.

ware that is used, and this noise is not necessarily without bias. In that case, increasing the computational resources may not further improve the results. As this depends on the specific situation, we leave this for future studies.

IV. DISCUSSION AND CONCLUSION

Training QBMs by gradient descent requires calculating the difference in statistics between the target and the model. In general, this is intractable because it involves computing exact Gibbs state expectation values. This has been shown to be QMA-hard [11], which means that even a quantum algorithm could take exponential time. We show that the β -VQE can be used as an efficient heuristic for obtaining the gradient in practice. When combined with the QBM training loop, we dubbed this the nested-loop training algorithm.

When the target is constructed from classical data, we find that the QBM can be trained using a low-rank ver-

sion of β -VQE. This is also observed for quantum data originating from low-temperature systems. For high-temperature quantum systems, a high rank is needed to achieve high fidelity. Yet, for the data considered here, we find numerically that a circuit depth scaling linearly with the system size is sufficient. We also find that a warm-start strategy for β -VQE can significantly reduce the overall computational cost. For these reasons, we think the nested-loop algorithm is a promising near-term approach to QBM training.

The nested-loop algorithm with two different model density matrices, being σ_w and $\rho_{\theta,\phi}$, may seem redundant, and one may wonder why the β -VQE is not used to represent the data directly. However, optimization of the β -VQE on the data density matrix directly requires computing the fidelity, and hence the overlaps between quantum states. This is intractable for large system sizes. The QBM serves as an intermediary, providing a local parameterized Hamiltonian that can be evaluated on a circuit efficiently. Similarly, the β -VQE provides the low-rank approximation necessary to train the QBM. Previous experiments with rank-one approximations for QBM training have revealed this leads to problematic level crossings that prohibit convergence. An example is shown in Appendix C. Conversely, for a rank-one target, it is often necessary to use higher rank approximations for the

QBM to converge. The β -VQE provides an ideal approximation where the rank can be freely chosen, and whose statistics can be efficiently computed by evaluation of a quantum circuit. The nested loop algorithm leaves the user with two density matrix representations of the target state. Depending on the purpose, either one can be used as a final approximation to the data. For quantum tomography the QBM state σ_w is most useful, revealing a possible candidate for an underlying model. Note that it might still be hard to compute σ_w even for a converged QBM. For the purpose of classification and generative tasks, one might directly use the β -VQE density $\rho_{\theta,\phi}$.

In this work we analyzed β -VQE [1] as a subroutine for preparing Gibbs states in the nested-loop training algorithm. There exists a plethora of near-term methods that could be used as alternatives for the inner loop. These include other ways to minimize the free energy [33–36], for example by preparing the thermofield double state [37, 38]. As this research field becomes increasingly rich, a systematic comparison of algorithms for Gibbs state preparation will become essential in the future.

ACKNOWLEDGMENTS

We thank Samuel Duffield and Kirill Plekhanov for fruitful discussions.

[1] J.-G. Liu, L. Mao, P. Zhang, and L. Wang, Solving quantum statistical mechanics with variational autoregressive networks and quantum circuits, *Machine Learning: Science and Technology* **2**, 025011 (2021).

[2] S. Lloyd, S. Garnerone, and P. Zanardi, Quantum algorithms for topological and geometric analysis of data, *Nature communications* **7**, 10138 (2016).

[3] Z. Zhao, J. K. Fitzsimons, and J. F. Fitzsimons, Quantum-assisted gaussian process regression, *Phys. Rev. A* **99**, 052331 (2019).

[4] M. Cerezo, A. Arrasmith, R. Babbush, S. C. Benjamin, S. Endo, K. Fujii, J. R. McClean, K. Mitarai, X. Yuan, L. Cincio, and P. J. Coles, Variational quantum algorithms, *Nature Reviews Physics* **3**, 625 (2021).

[5] M. Benedetti, E. Lloyd, S. Sack, and M. Fiorentini, Parameterized quantum circuits as machine learning models, *Quantum Science and Technology* **4**, 043001 (2019).

[6] J. Tilly, H. Chen, S. Cao, D. Picozzi, K. Setia, Y. Li, E. Grant, L. Wossnig, I. Rungger, G. H. Booth, and J. Tennyson, The variational quantum eigensolver: A review of methods and best practices, *Physics Reports* **986**, 1 (2022), the Variational Quantum Eigensolver: a review of methods and best practices.

[7] M. H. Amin, E. Andriyash, J. Rolfe, B. Kulchytskyy, and R. Melko, Quantum boltzmann machine, *Phys. Rev. X* **8**, 021050 (2018).

[8] M. Benedetti, J. Realpe-Gómez, R. Biswas, and A. Perdomo-Ortiz, Quantum-assisted learning of hardware-embedded probabilistic graphical models, *Phys. Rev. X* **7**, 041052 (2017).

[9] M. Kieferová and N. Wiebe, Tomography and generative training with quantum boltzmann machines, *Phys. Rev. A* **96**, 062327 (2017).

[10] H. J. Kappen, Learning quantum models from quantum or classical data, *Journal of Physics A: Mathematical and Theoretical* **53**, 214001 (2020).

[11] S. Bravyi, A. Chowdhury, D. Gosset, and P. Wocjan, On the complexity of quantum partition functions (2021), arXiv:2110.15466 [quant-ph].

[12] G. E. Hinton, Training products of experts by minimizing contrastive divergence, *Neural Computation* **14**, 1771 (2002).

[13] X.-Y. Guo, S.-S. Li, X. Xiao, Z.-C. Xiang, Z.-Y. Ge, H.-K. Li, P.-T. Song, Y. Peng, Z. Wang, K. Xu, P. Zhang, L. Wang, D.-N. Zheng, and H. Fan, Variational quantum simulation of thermal statistical states on a superconducting quantum processor, *Chinese Physics B* **32**, 010307 (2023).

[14] C. Zoufal, A. Lucchi, and S. Woerner, Variational quantum boltzmann machines, *Quantum Machine Intelligence* **3** (2021).

[15] E. R. Anschuetz and Y. Cao, Realizing quantum boltzmann machines through eigenstate thermalization (2019).

[16] L. Coopmans, Y. Kikuchi, and M. Benedetti, Predicting gibbs-state expectation values with pure thermal shadows, *PRX Quantum* **4**, 010305 (2023).

[17] N. Wiebe and L. Wossnig, Generative training of quantum boltzmann machines with hidden units (2019), arXiv:1905.09902 [quant-ph].

[18] M. Kieferova, O. M. Carlos, and N. Wiebe, Quantum generative training using rényi divergences (2021), [arXiv:2106.09567 \[quant-ph\]](https://arxiv.org/abs/2106.09567).

[19] D. H. Ackley, G. E. Hinton, and T. J. Sejnowski, A learning algorithm for boltzmann machines*, *Cognitive Science* **9**, 147 (1985).

[20] H. E. Haber, Notes on the matrix exponential and logarithm (2018).

[21] N. Zhang, S. Ding, J. Zhang, and Y. Xue, An overview on restricted boltzmann machines, *Neurocomputing* **275**, 1186 (2018).

[22] E. Y. Loh, J. E. Gubernatis, R. T. Scalettar, S. R. White, D. J. Scalapino, and R. L. Sugar, Sign problem in the numerical simulation of many-electron systems, *Phys. Rev. B* **41**, 9301 (1990).

[23] G. Pan and Z. Y. Meng, Sign problem in quantum monte carlo simulation (2022), [arXiv:2204.08777 \[cond-mat.str-el\]](https://arxiv.org/abs/2204.08777).

[24] M. Germain, K. Gregor, I. Murray, and H. Larochelle, Made: Masked autoencoder for distribution estimation (2015), [arXiv:1502.03509 \[cs.LG\]](https://arxiv.org/abs/1502.03509).

[25] J. R. McClean, S. Boixo, V. N. Smelyanskiy, R. Babbush, and H. Neven, Barren plateaus in quantum neural network training landscapes, *Nature Communications* **9**, 4812 (2018).

[26] S. Mohamed, M. Rosca, M. Figurnov, and A. Mnih, Monte carlo gradient estimation in machine learning (2020), [arXiv:1906.10652 \[stat.ML\]](https://arxiv.org/abs/1906.10652).

[27] V. V. Shende, I. L. Markov, and S. S. Bullock, Minimal universal two-qubit controlled-not-based circuits, *Phys. Rev. A* **69**, 062321 (2004).

[28] While the specifics of the update scheme do not noticeably change the quality of the final result, we find that they do have a large impact on the number of outer loop iterations needed to get there. Fast convergence was usually achieved with a variable learning rate that is increased by 1% after every iteration as long as the cost function decreased, and halved if the cost function increased, combined with some momentum.

[29] G. Tkačik, O. Marre, D. Amodei, E. Schneidman, W. Bialek, and M. J. Berry, II, Searching for collective behavior in a large network of sensory neurons, *PLOS Computational Biology* **10**, 1 (2014).

[30] Y.-C. Liang, Y.-H. Yeh, P. E. M. F. Mendonça, R. Y. Teh, M. D. Reid, and P. D. Drummond, Quantum fidelity measures for mixed states, *Reports on Progress in Physics* **82**, 076001 (2019).

[31] J. Preskill, Quantum Computing in the NISQ era and beyond, *Quantum* **2**, 79 (2018).

[32] M. A. Nielsen and I. L. Chuang, Quantum computation and quantum information, *Phys. Today* **54**, 60 (2001).

[33] G. Verdon, J. Marks, S. Nanda, S. Leichenauer, and J. Hidary, Quantum hamiltonian-based models and the variational quantum thermalizer algorithm (2019), [arXiv:1910.02071 \[quant-ph\]](https://arxiv.org/abs/1910.02071).

[34] J. Foldager, A. Pesah, and L. K. Hansen, Noise-assisted variational quantum thermalization, *Scientific reports* **12**, 3862 (2022).

[35] Y. Wang, G. Li, and X. Wang, Variational quantum gibbs state preparation with a truncated taylor series, *Phys. Rev. Appl.* **16**, 054035 (2021).

[36] M. Consiglio, J. Settino, A. Giordano, C. Mastroianni, F. Plastina, S. Lorenzo, S. Maniscalco, J. Goold, and T. J. G. Apollaro, Variational gibbs state preparation on nisq devices (2023), [arXiv:2303.11276 \[quant-ph\]](https://arxiv.org/abs/2303.11276).

[37] J. Wu and T. H. Hsieh, Variational thermal quantum simulation via thermofield double states, *Phys. Rev. Lett.* **123**, 220502 (2019).

[38] J. Martyn and B. Swingle, Product spectrum ansatz and the simplicity of thermal states, *Phys. Rev. A* **100**, 032107 (2019).

Appendix A: Salamander retina data

The classical data set we consider is presented in [29]. The set consists of data on 160 neurons on the retina of a salamander that were exposed to 297 repeats of a natural movie. For every 20ms it was recorded for each neuron whether or not they fired. From the full data set, we select a subset of neurons with high firing rates and mutual information. The first 30 repeats of the movie are used as a training set, and all other repeats are grouped in bins of 10 to form test sets.

As shown in [10], the QBM outperforms the classical BM on this data set. We reproduce these results for the QBM trained with the nested-loop algorithm. The results are shown in Figure 7. The QBM density matrix σ_w converges to a rank-one solution where the ground state accurately represents the data probability distribution, with a KL divergence of 0.01 (blue cross). The classical BM achieves a KL of 0.021 (red cross). The QBM also generalized better with a lower KL divergence on all test sets (blue bars) compared to the classical BM (red bars).

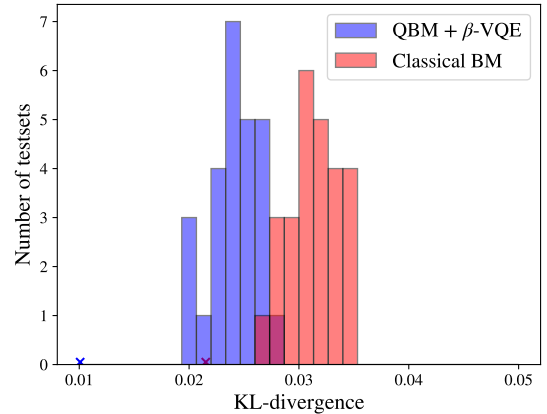


FIG. 7. KL divergence for both the QBM and classical BM on the salamander retina data set.

Appendix B: Circuit-depth analysis

In this section, we assume the QBM in the outer loop is fixed to the Heisenberg XXZ model in Eq. (14) with $\beta = 1$. We then analyze the effect of circuit depth in β -VQE which, as a reminder, is executed in the inner loop to approximate the QBM.

We use the exact gradient in Eq. (7) and increase the circuit depth from 3 to 8 layers. We compute the Uhlmann-Jozsa fidelity in Eq. (13) between the β -VQE and the QBM. The results are shown in Figure 8. Clearly, deeper circuits can achieve higher fidelity. We emphasize however that increasing the circuit depth is computationally expensive as the resulting circuits contain more parameters to train. A circuit depth of 8 is sufficient to obtain $F > 0.98$.

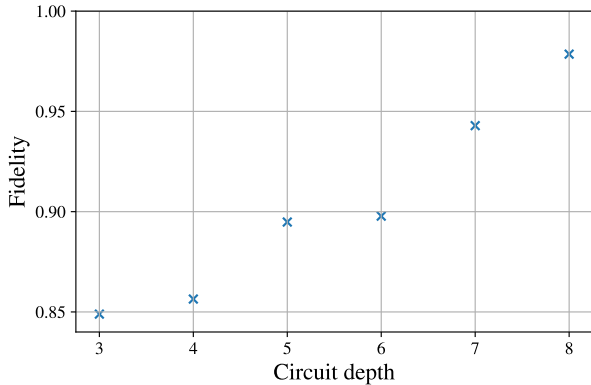


FIG. 8. Fidelity between the QBM and the target for different circuit depths.

Appendix C: Rank-one QBM training

For targets encoding classical data, the QBM usually converges to a rank-one solution. Thus, one may wonder if it is possible to train the QBM using only the ground state to approximate the gradient. This would provide an opening to using various methods of ground state approximation. We find that using a rank-one approximation does not work in general due to problematic level crossings. As the QBM converges, level crossings between the ground state and the first excited state can occur. Consequentially, the ground state approximation of the gradient changes drastically between two iterations. This is troublesome if the gradient after the level crossing again directs the model back over the level crossing. In such a case, one can only converge closer to the exact point of degeneracy, and at that point, it is not possible to train the QBM further using the ground state approximation. Such a case is plotted in Figs. 9 and 10.

One might see the resemblance between the spikes in the norm of the gradient in Fig. 9 (inset) and the two spikes in Fig. 1 (inset). However, they are due to different events. For rank-one training in Fig. 9 the spikes coincide with the level crossings in Fig. 10. Instead, for the truncated-rank β -VQE in Fig. 1 there is always a gap as shown in Fig. 11. In this case the spikes are due to the high momentum and variable learning rate that we use during training. These settings accelerate training, especially for rank-one targets. But, sometimes, they cause the QBM to overshoot the optimal point, causing the spikes.

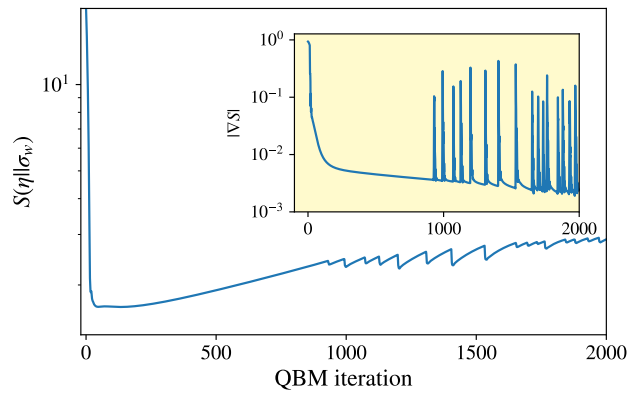


FIG. 9. Convergence of the QBM trained using a rank-one approximation and classical target data.

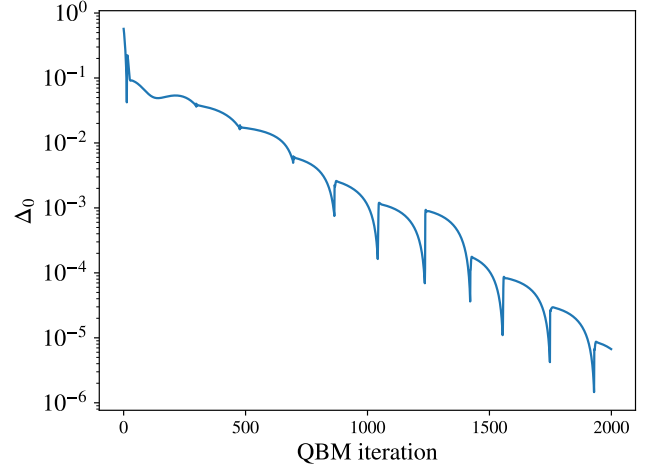


FIG. 10. Spectral gap between the ground state and first excited state of σ_w during QBM training using a rank-one approximation.

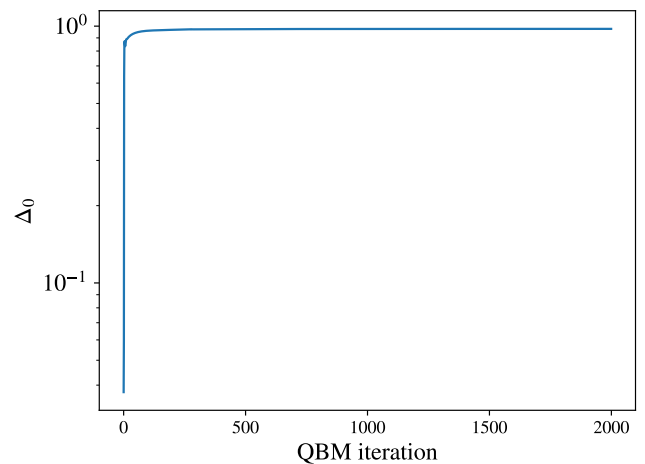


FIG. 11. Spectral gaps of σ_w during QBM training using the nested-loop algorithm.